Natural mechanism of the broadened Snoek relaxation profile in ternary body-centered-cubic alloys

Liming Yu, Fuxing Yin, and Dehai Ping
Innovative Materials Engineering Laboratory, National Institute for Materials Science, Tsukuba 305-0047, Japan
(Received 4 January 2007; revised manuscript received 6 March 2007; published 15 May 2007)

The natural mechanism of the broadened Snoek relaxation peak in the ternary bcc alloy system has been investigated by an embedded-cell model of statistical mechanical treatment. In this method, interstitial sites of different geometries (octahedral, tetrahedral, etc.) in bcc crystals are considered and further distinguished by element species and atomic arrangements within their first shell of the neighbors. Following these preconditions, the interstitial site occupancies, the spatial configurations, and the transition probabilities of the interstitial atoms are concretely calculated for the ternary bcc alloy system, and all possible elementary relaxation processes contributing to the broadened Snoek peak are physically described with the determined activation energy and peak temperature for each elementary process. Using this approach for Snoek peak deconvolution, the broadened Snoek peak of the ternary bcc alloy can be resolved into several elementary Debye peaks, which correspond to the concrete relaxation mechanism. In the present study, this method is successfully applied to analyze the natural mechanism of experimentally observed Snoek relaxation in Nb-Ti-O systems.

DOI: 10.1103/PhysRevB.75.174105 PACS number(s): 62.40.+i, 67.80.Mg, 61.50.Ah

I. INTRODUCTION

Snoek relaxation[1] is the mechanical relaxation phenomenon caused by the stress-induced redistribution of octahedral interstitial atoms in body-centered-cubic (bcc) metals. Although this is one of the best-understood relaxation phenomena among a number of anelastic effects in crystalline solids, the atom transition mechanism of this process has not been unambiguously identified. Especially in the ternary alloys,[2,3] complex interactions exist among interstitial atoms (I) and host- (M) and substitutional-metal (S) atoms. These interactions will markedly influence the anelastic relaxation processes, which are controlled by the thermally activated transitions of the interstitial atoms between the equivalent interstitial sites. As a result, Snoek relaxation in ternary bcc alloys usually shows complex characteristics[2] such as broadening, asymmetry or even new peak formation, etc. In the past 50 years, many ternary bcc alloys have been investigated in order to clarify the nature of the complex Snoek relaxation. However, the explanations were quite contradictory and limited.[4]

Broadened Snoek peaks have also been observed in concentrated binary bcc alloys, such as Ta-O (Ref. 5) or Nb-O (Refs. 6 and 7) systems. Early studies of the broadened relaxation peaks were attributed to the stress-induced transitions of interstitial atoms in pairs, triplets, or higher order clusters. This interpretation is the so-called S-kI interaction model ($k=1$, 2, 3, or 4). Botta *et al.* and Florencio *et al.* extended this model into Nb-Zr-O and Nb-Ti-O ternary systems.[8,9] However, the deduced relaxation parameters, such as the peak temperature and the activation energy, exhibited qualitative consistency but quantitative disagreement. These results seem to be rather speculative.

Early investigations on the effect of substitutional solutes in ternary alloy systems were focused on Fe-Mn-N alloys,[10] and then extended to Fe-Mn(Cr)-C systems[11] and alloys based on group-V transition metals (V, Nb, and Ta).[12,13] In most of these studies, distortion of the relaxation spectrum was attributed to the interaction between substitutional and interstitial solute atoms, which was referred to as the "S-I" interaction.[14] Some of the characteristic features can be qualitatively explained in terms of local attractive S-I interaction based on the general theory given by Nowick and Heller[15] and Koiwa.[16] These theoretical approaches were made with the assumption that all substitutional atoms exist as isolated single atoms. This is only an adequate approximation for ternary alloy systems with a highly diluted substitutional solute.

With the increase of substitutional solutes concentration, more than one substitutional atoms may occupy the nearest-neighbor lattice sites of the octahedral interstice. To account for this case, the interaction between interstitial atoms and the adjacent substitutional solutes, i.e., the so-called jS-I interaction ($j=0,1,\ldots 6$), has been considered and emphasized in recent investigations. This viewpoint has been used to interpret the complex Snoek effect in concentrated ternary alloys, such as Nb-V(Mo,Zr)-O(N),[17–20] Fe-Cr(Al,Mn)-C(N),[21–23] Ta-Re-O,[24] etc. In this approach, the transition of interstitial atoms was assumed to be a confined orientation in one octahedral cell. However, as shown in Fig. 1, the actual situation is more complicated since a Snoek transition of interstitial atoms must occur between two adjacent octahedral cells. Therefore, a certain type of elementary relaxation process jS-I should possess different relaxation parameters since the multiform spatial correlation may exist in this transition.

Undoubtedly, complex Snoek relaxation in a ternary alloy system contains several elementary relaxation processes. However, the assignment of the constituent peaks to individual jump processes is generally invalid if it does not reflect a concrete and reasonable physical mechanism. Therefore, the problem-solving method should be first, to analyze all possible elementary relaxation processes using the reasonable physical models and, second, to separate the total relaxation profile into the component relaxation peaks.

A Snoek relaxation process mainly depends on the occupancies of the octahedral interstitial sites and on the transi-

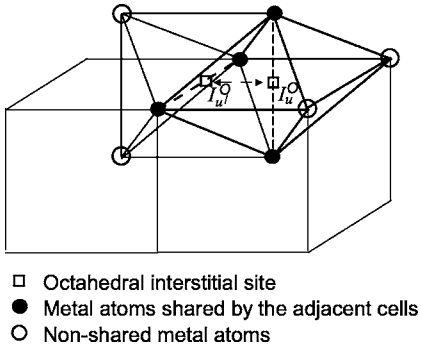

FIG. 1. The schematic process of a Snoek relaxation. In this procedure, the interstitial atom transits between two adjacent octahedral cells, i.e., jumps from octahedral site I_u^O to $I_{u'}^O$. It also can be seen that four metal atoms are shared by the adjacent cells. Here, the superscript O represents the octahedral interstice.

tion status of the interstitial atoms. These factors are controlled not only by the site energies but also by the complex interactions between interstitial atoms and matrix metal atoms.[25] Thus, the description of Snoek relaxation in ternary alloy system is usually tackled under simplified assumptions,[26] such as ideal intersolubility between the host metal and substitutional solutes, random distribution among the lattices site, short-range interaction between interstitial atoms, etc. Recently, an embedded-cell model,[27–29] based on the statistical mechanical method,[30–32] was developed to deal with the interstitial atoms' behavior in ternary interstitial alloys. In this model, the interstitial sites of different geometries (octahedral, tetrahedral, etc.) are considered and further distinguished by the chemical composition and atomic arrangement in the first shell of the neighboring metal atoms, and then, the interstitial atoms' behavior is controlled by the composition of both the embedding matrix and the first shell formed by metal atoms. This model has been successfully applied to calculate the diffusion and solution heat of hydrogen (and deuterium) interstitial in ternary fcc or bcc system.[28,29] Biscarini *et al.* applied this method to deal with the anelastic relaxation behavior of interstitial solutes in ternary systems, but the estimation was quite qualitative and poorly operable.[26]

In the present work, we extend this embedded-cell model to analyze the broadened Snoek relaxation behavior in bcc ternary alloys. The influence of the short-range ordering, the spatial correlation of lattice sites, and the site-dependent activation energies will be simultaneously taken into account. The main objective is to acquire a clearer picture of the concrete mechanisms that contribute to the Snoek relaxation in such alloy systems. In addition, this investigation could provide a useful method for the description and understanding of anelastic behaviors and diffusion mechanisms related to interstitial atoms in ternary alloy systems.

This paper is organized as follows. In Sec. II the static distribution and the spatial correlation of the interstitial atoms at octahedral sites in ternary bcc systems are calculated in detail. This information is then used to analyze the possible elementary relaxation processes, which correspond to the concrete transition configurations. Then, in Sec. III the dynamic transitions of these elementary processes and their contributions to the whole Snoek relaxation profile are treated using a fitting procedure. Following this analysis, the complicated relaxation spectrum can be reasonably resolved into elementary relaxation peaks. Finally, as an example, this method is applied to analyze the Snoek relaxation in Nb-Ti-O alloys with different Ti compositions (Sec. IV). Nb-Ti-O alloys were chosen for the following reasons. Unlike other interstitial atoms such as nitrogen, carbon, etc., oxygen atoms have a high solubility in Nb-Ti-based alloys.[33] Recent research[34] has shown that practical Snoek-type high-damping alloys can be realized in this alloy. Nb and Ti have approximately the same molar volume,[29] so elastic interaction between the metal atoms can be neglected. Furthermore, it has been established that the local order parameter (σ) in Nb-Ti alloys was rather low[35] (σ ranging between 0.1 and 0.15), which indicated that this alloy could be approximately treated as a random system. These structural factors have a good coincidence with the assumptions required by the statistical mechanical method.

II. STATIC DISTRIBUTION OF THE INTERSTITIAL ATOMS IN THE TERNARY bcc SYSTEM

The present calculations will be made with the following assumptions.

(i) Interstitial atoms occupy only the octahedral interstices under thermal equilibrium conditions.

(ii) The interstitial atoms are allowed to transit only to the nearest-neighbor octahedral sites

(iii) In the absence of an external stress, the distribution of interstitial atoms over various sites is that of thermal equilibrium at any temperature.

A. Distribution of interstitial sites

According to the assumption of the embedded-cell model, in a random bcc alloy $A_{1-y}B_y$, seven octahedral interstitial sites I_u^O ($u=0,1,2,\ldots,6$) and five tetrahedral sites I_v^T ($v=0,1,\ldots,4$) can be distinguished, depending on the chemical composition and atomic arrangement within the first shell (as shown in Table I). Here, u or v represents the number of substitutional atoms occupying the nearest-neighbor lattice sites of the octahedral or tetrahedral interstice, respectively. Thus, the first shell of neighbors can be considered to be a cell of composition $A_{6-u}B_u$ or $A_{4-v}B_v$. The number of distinguishable sites becomes 24 if the symmetry features associated with the distribution of substitutional solutes among the nearest lattice sites are also take into account. In an ideal system ($\sigma=0$), the atoms are randomly distributed among the lattice sites and the fraction P_u^O (or P_v^T) of a certain type of interstitial site I_u^O (or I_v^T) can be given by a binomial distribution function. The expressions of P_u^O and P_v^T in an ideal system are also listed in Table I. Under thermal equilibrium conditions, interstitial atoms are assumed to occupy only the octahedral interstices.

However, in most actual alloy systems, short-range ordered or ordered effects have been observed. The detailed derivation of tetrahedral cluster probability $P_v^T(\sigma)$ was given

TABLE I. Distinguishable octahedral and tetrahedral interstitial sites (I_u^O and I_v^T) in a bcc alloys ($A_{1-y}B_y$) and the associated fractions (P_u^O and P_v^T) in randomly status (σ=0). (○—A atoms and ●—B atoms; the superscript O and T represent the octahedral and tetrahedral interstices, respectively.)

	Octahedral Site			Tetrahedral Site		
u or v	Cell Configuration $A_{6-u}B_u$	Interstitial Site Type (I_u^O)	Site Fraction (P_u^O)(σ=0)	Cell Configuration $A_{4-v}B_v$	Interstitial Site Type (I_v^T)	Site Fraction (P_v^T)((σ=0)
0	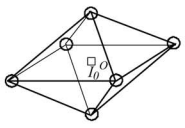	I_0^O	$\frac{1}{3}(1-y)^6$	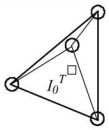	I_0^T	$\frac{2}{3}(1-y)^4$
1	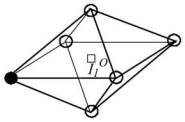	I_1^O	$2(1-y)^5 y$	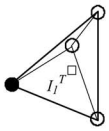	I_1^T	$\frac{8}{3}(1-y)^3 y$
2	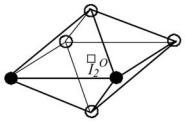	I_2^O	$5(1-y)^4 y^2$	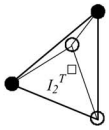	I_2^T	$4(1-y)^2 y^2$
3	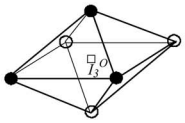	I_3^O	$\frac{20}{3}(1-y)^3 y^3$	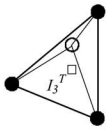	I_3^T	$\frac{8}{3}(1-y)y^3$
4	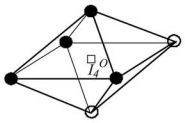	I_4^O	$5(1-y)^2 y^4$	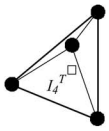	I_4^T	$\frac{2}{3}y^4$
5	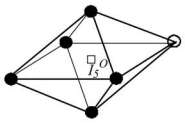	I_5^O	$2(1-y)y^5$			
6	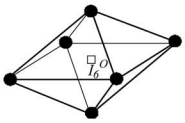	I_6^O	$\frac{1}{3}y^6$			

in Ref. 29, in which the local order parameter σ ($\sigma \neq 0$) was considered. Here, we extend this method to calculate the fractions of octahedral cells. As shown in Fig. 2, an octahedral cell contains two sub-cells: a tetrahedron cell and a double-atom cell. The probability of finding an A_6 cell in the system is thus given by

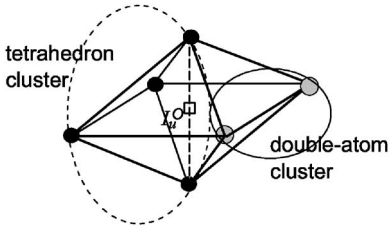

FIG. 2. Structure of a octahedral cell in bcc system. It can be treated as a clusters chain in which contain a tetrahedron cell and a double-atom cell.

$$P_0^O(\sigma) = P_0{}^T(\sigma)P_A P_{AA}. \tag{1a}$$

The analogous expressions for the formation of the other octahedral cells are

$$P_1^O(\sigma) = P_0^T(\sigma)P_A P_{AB} + P_0^T(\sigma)P_B P_{BA} + P_1^T(\sigma)P_A P_{AA}, \tag{1b}$$

$$P_2^O(\sigma) = P_0^T(\sigma)P_B P_{BB} + P_1^T(\sigma)P_A P_{AB} + P_1^T(\sigma)P_B P_{BA} + P_2^T(\sigma)P_A P_{AA}, \tag{1c}$$

$$P_3^O(\sigma) = P_1^T(\sigma)P_B P_{BB} + P_2^T(\sigma)P_A P_{AB} + P_2^T(\sigma)P_B P_{BA} + P_3^T(\sigma)P_A P_{AA}, \tag{1d}$$

$$P_4^O(\sigma) = P_4^T(\sigma)P_A P_{AA} + P_3^T(\sigma)P_A P_{AB} + P_3^T(\sigma)P_B P_{BA} + P_2^T(\sigma)P_B P_{BB}, \tag{1e}$$

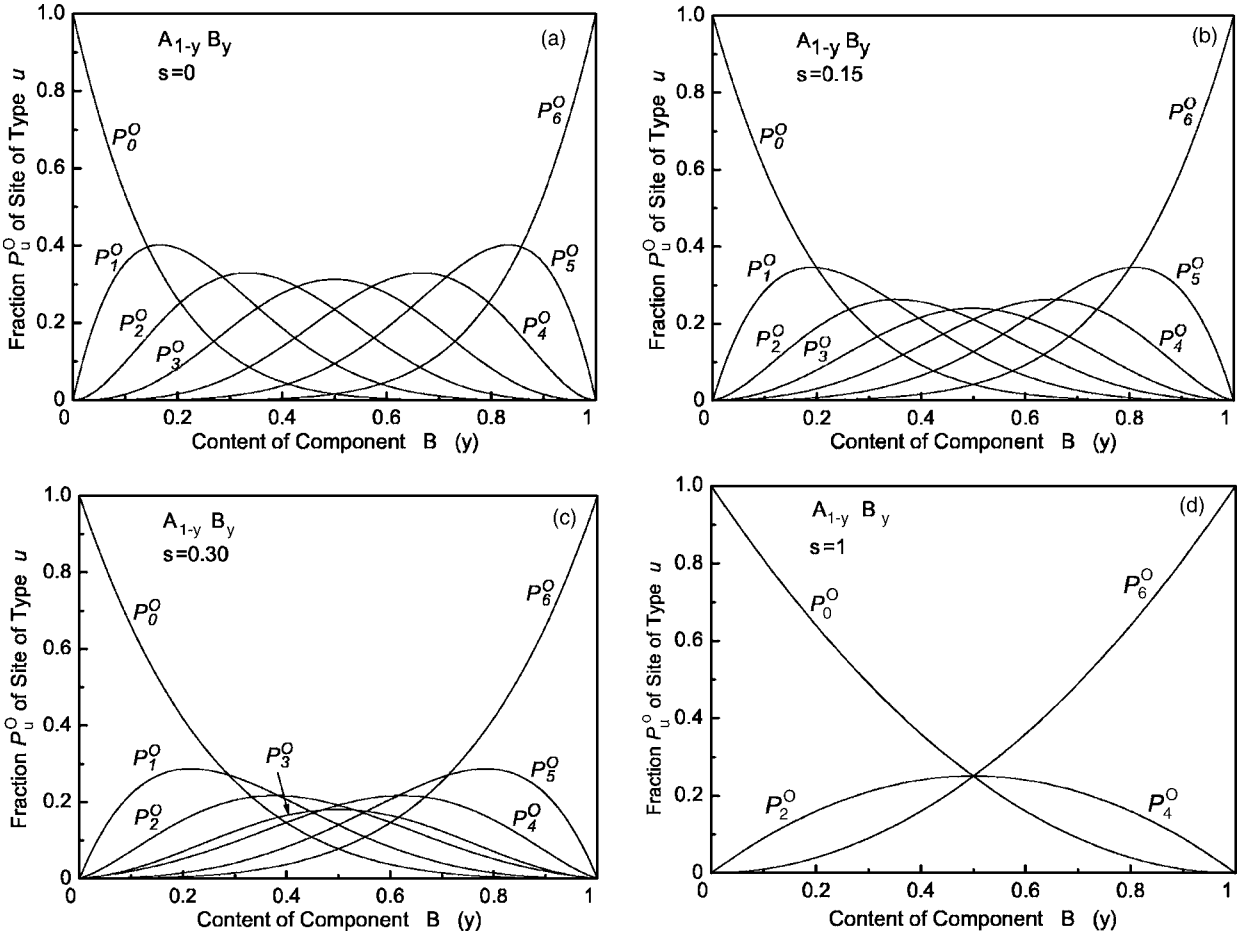

FIG. 3. Friction P_u^O of octahedral sites of a short range ordered or ordered ternary bcc system. The sites were distinguished by the different chemical compositions in the first shell of neighbors: (a) $\sigma=0$ (ideal random system), (b) $\sigma=0.15$, (c) $\sigma=0.30$, and (d) $\sigma=1$ (ordered system).

$$P_5^O(\sigma) = P_4^T(\sigma)P_A P_{AB} + P_4^T(\sigma)P_B P_{BA} + P_3^T(\sigma)P_B P_{BB}, \tag{1f}$$

$$P_6^O(\sigma) = P_4^T(\sigma)P_B P_{BB}, \tag{1g}$$

where P_A or P_B is the probability of the lattice atoms, and $P_{AA(B)}$ is the probability of finding an A (or B) atom as nearest neighbor of another A atom. The fractions of different octahedral sites P_u^O in a short-range ordered and ordered system are shown in Fig. 3. It can be seen that the cell fractions are strongly influenced by the amount of short-range order σ. In an ordered system, i.e., $\sigma=1$, four kinds of octahedral cells exist: A_6, B_6, and the transitional cells A_4B_2 and A_2B_4 between A_6 and B_6.

B. Spatial correlation between adjacent octahedral interstitial sites

Pairs of adjacent octahedral interstitial sites are shown in Fig. 1 together with the cells of their nearest neighbor metal atoms. It can be seen that four metal atoms are shared by adjacent cells. Due to this geometric restriction, some jumping routes of interstitial atoms are precluded. For example, an interstitial atom in A_6 site cannot transit into an adjacent B_6 interstitial site, since the probability of finding a B_6 site next to an A_6 site is zero. In order to calculate the probability factors for an interstitial atoms' transition from one interstitial site to another, spatial short-distance correlations among different types of sites need to be known as a function of the alloy composition y. For this purpose, the conditional probability $q_{uu'}^O$ that, given an octahedral interstitial site of type u, another site selected among the sites adjacent to the first one is of type u', needs to be calculated. The expressions[26] for $q_{uu'}^O$ are listed in Table II, where empty spaces mean that the probability $q_{uu'}^O$ is equal to zero. All possible configurations of adjacent octahedral sites in a bcc ternary system have been taken into account in Table II. One may notice that the transition of interstitial atoms between adjacent octahedral sites can only occur if the difference value between u and u' is less than or equal to 2, i.e., $|u-u'| \leqslant 2$.

C. Occupancies of interstitial atoms in the octahedral interstitial sites

The interstitial atom concentration in a certain octahedral site c_u^O, i.e., the number of interstitial atoms occupying a given type of site (I_u^O) divided by the total number of the

TABLE II. Conditional probabilities $q^O_{uu'}$, which means finding an octahedral site of type u' as the nearest neighbor of site of type u as a function of the ternary system composition.

$q_{uu'}$	I^O_0	I^O_1	I^O_2	I^O_3	I^O_4	I^O_5	I^O_6
$I^O_{0'}$	$(1-y)^2$	$2(1-y)y$	y^2				
$I^O_{1'}$	$\frac{1}{4}(1-y)^2$	$\frac{1}{2}(1-y)y+\frac{3}{4}(1-y)^2$	$\frac{3}{2}(1-y)y+\frac{1}{4}y^2$	$\frac{3}{4}y^2$			
$I^O_{2'}$	$\frac{1}{16}(1-y)^2$	$\frac{1}{8}(1-y)y+\frac{1}{2}(1-y)^2$	$\frac{7}{16}(1-y)^2+\frac{1}{16}y^2+(1-y)y$	$\frac{7}{8}(1-y)y+\frac{1}{2}y^2$	$\frac{7}{16}y^2$		
$I^O_{3'}$		$\frac{3}{16}(1-y)^2$	$\frac{3}{8}(1-y)y+\frac{1}{8}(1-y)^2$	$\frac{3}{16}(1-y)^2+\frac{3}{16}y^2+\frac{5}{4}(1-y)y$	$\frac{3}{8}(1-y)y+\frac{5}{8}y^2$	$\frac{3}{16}y^2$	
$I^O_{4'}$			$\frac{7}{16}(1-y)^2$	$\frac{7}{8}(1-y)y+\frac{1}{2}(1-y)^2$	$\frac{1}{16}(1-y)^2+\frac{7}{16}y^2+(1-y)y$	$\frac{1}{8}(1-y)y+\frac{1}{2}y^2$	$\frac{1}{16}y^2$
$I^O_{5'}$				$\frac{3}{4}(1-y)^2$	$\frac{3}{2}(1-y)y+\frac{1}{4}(1-y)^2$	$\frac{1}{2}(1-y)y+\frac{3}{4}y^2$	$\frac{1}{4}y^2$
$I^O_{6'}$					$(1-y)^2$	$2(1-y)y$	y^2

octahedral interstitial sites, mainly depends on the site energy e^O_u. In a diluted interstitial solute system, the interaction between interstitial atoms can be neglected and c^O_u can be described using the Maxwell-Boltzmann statistical equation. While in a concentrated system, the Fermi-Dirac statistics become more suitable as has been discussed by Kirchheim,[36] since the interstitial atom interactions can be taken into account by adding a concentration-dependent contribution $f(c)$ to the site energy e^O_u,

$$c^O_u = \frac{P^O_u}{1+\exp\{[e^O_u + f(c)]/kT\}} \quad (u=0,1,\ldots,6). \tag{2}$$

In Eq. (2), the interaction $f(c)$ is assumed to depend only on the total interstitial atoms concentration C with the boundary condition $C=\Sigma^6_{u=0}c^O_u$ for reasons discussed in Refs. 28 and 32.

The site energy (e^O_u) of an interstitial atom strongly depends on the chemical affinity (Λ) between interstitial atoms and the nearest neighbor metal atoms, and on the elastic interaction of the local strain field (ε) of a cell in a matrix alloy, i.e.,

$$e^O_u = e^O_u(\Lambda) + e^O_u(\varepsilon). \tag{3}$$

Here, an embedded-cell method[29,32] was applied to calculate the site energy (e^O_u). An octahedral cell $A_{6-u}B_u$ can be treated as an alloy with a local concentration $y'=u/6$, and embedded into the matrix alloy $A_{1-y}B_y$ with the concentration y (as shown in Fig. 4). The site energy is assumed to depend predominantly on the difference between the local cell component and the matrix. If a cell is embedded in an alloy with the same average composition as the cell itself, for example, an A_3B_3 cell in an $A_{0.5}B_{0.5}$ alloy, this cell is a so-called free cell. The site energy of the free cell, denoted $e^{O^*}_u[e^{O^*}_u = e^{O^*}_u(\Lambda)+e^{O^*}_u(\varepsilon)]$, is used as the reference value.

As shown in Ref. 28, prior to and after embedment, the difference of the cell volume (ΔV) can be expressed as

$$\Delta V = (1-y)V_A + yV_B - \frac{(6-u)V_A + uV_B}{6} \quad (u=0,1,\ldots,6), \tag{4}$$

in which V_A and V_B are the cell volumes of A_6 and B_6 in the pure metals. Thus, the elastic interaction part of the site energy $[e^O_u(\varepsilon)]$ of an octahedral interstitial site in a ternary bcc system can be given by

$$e^O_u(\varepsilon) = e^{O^*}_u(\varepsilon) - (1-D)\Omega\Delta V. \tag{5}$$

Here, Ω is the bulk modulus of the alloy. The parameter $D\in[0,1]$ represents the force constant between nearest-neighbor atoms.

The chemical interaction should be roughly proportional to the different "affinity" between the interstitial-substitutional solute $(S\text{-}I)$ and the interstitial-host element $(M\text{-}I)$. A quantitative measure of the affinity force of interstitial atoms with matrix atoms is not generally available, but a good approximation might be given by the difference of heat of formation (ΔH^f) of the steady-state compound,[37] i.e., ΔH^f_{SI} and ΔH^f_{HI}. Analogous to Eq. (5), we have

$$e^O_u(\Lambda) = e^{O^*}_u(\Lambda) - (y-u/6)\Lambda, \tag{6}$$

where $\Lambda=\Delta H^f_{HI}-\Delta H^f_{SI}$.

Here, we apply this procedure to the Nb-Ti-O alloys. The parameters used in these calculations are listed in Table. III. In this case, the energy of the free cell $e^{O^*}_u$ is assumed to be zero as a reference value. NbO and TiO_2 oxides are used in the calculation of Λ. The calculated values of e^O_u are plotted versus alloy composition in Fig. 5.

As shown in Fig. 5, the energy of a given site depends on the average composition of the embedding alloy matrix, and the Ti_6 site is the most energetically favorable for oxygen occupancy compared to other sites. Since Nb and Ti have similar atomic radii, the elastic interaction is negligible. The main contribution to the site energy is due to the chemical affinity force. In this system, the Ti substitutional solute has a higher affinity for oxygen than the host element Nb; there-

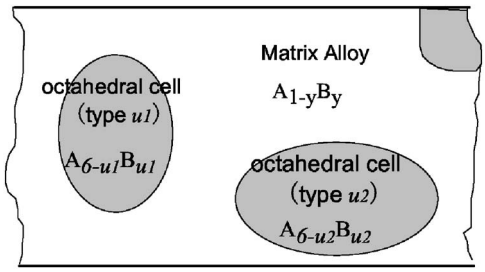

FIG. 4. Schematic representation of the embedded-cell model. An octahedral cell $A_{6-u}B_u$ was treated as an alloy with local concentration $y'=u/6$ and embedded into the matrix alloy $A_{1-y}B_y$ with the concentration y.

fore, oxygen atoms tend to distribute in the octahedral cells that contain more Ti solutes.

Substituting Eqs. (3), (5), and (6) into Eq. (2) leads to a set of nonlinear equations in the unknown quantities c_u^O. With the boundary condition $C=\Sigma_{u=0}^6 c_u^O$, the normalized site concentrations c_u^O/C, calculated as a function of Ti content (y) in $Nb_{(1-y)}Ti_y$ for different temperatures, are shown in Fig. 6.

It can be seen that interstitial oxygen atoms preferentially occupy the octahedral interstitial sites, which have nearest-neighbor Ti substitutional atoms due to more favorable site-dependent energies. For example, in the Nb-0.75Ti-1.5O (at. %) alloy, the fraction of octahedral cell Nb_6 is 96.68%; however, only 33.35% of oxygen atoms distribute over these cells. Most oxygen atoms occupy the cells of the types Nb_5Ti and Nb_4Ti_2, which contain one and two Ti atoms, respectively. Therefore, substitutional Ti solutes will markedly influence the Snoek relaxation behavior in the Nb-Ti-O ternary system, even if the concentration of Ti is rather low.[38] At higher temperature [Figs. 6(b) and 6(c)], the occupancies of higher-energy sites become appreciable and may contribute to the anelastic relaxation performance. As a result, the Snoek peak will be broadened, asymmetric, or even new peaks may appear, especially in the case where a local attractive interaction exists between the substitutional solutes and the interstitial atoms.

III. DYNAMIC TRANSITION OF INTERSTITIAL ATOMS AND SNOEK RELAXATION PROFILE

So far, the static distribution of interstitial atoms in different octahedral interstitial sites in a ternary bcc system has been considered. As previously mentioned, a Snoek relaxation results from the stress-induced transitions of interstitial atoms between the adjacent octahedral interstitial sites, i.e., $\Sigma_u I_u^O \rightarrow I_{u'}^O$. In order to get a complete picture of the interstitial atoms relaxation, the activation energy of each elementary jump ($I_u^O \rightarrow I_{u'}^O$) has to be determined.

A. Transition activation energy of interstitial atoms between adjacent octahedral sites

The potential energy for interstitial atoms migrating over adjacent octahedral sites ($I_u^O \rightarrow I_{u'}^O$) has been illustrated schematically in Fig. 7. The saddle-point energy of the interstitial atoms' jump ($Q_{uu'}$) appears at the tetrahedral interstitial site I_v^T between two adjacent octahedral sites.[14,39] This tetrahedral site is surrounded by four nearest-neighbor lattice atoms (denoted by 1, 2, 3, and 4 in Fig. 7), which are shared by the adjacent octahedral cell. Therefore, the saddle-point energy $Q_{uu'}$ can be treated as the tetrahedral site energy e_v^T, and the activation energy $H_{uu'}$ can be calculated by the following relation:

$$H_{uu'} = Q_{uu'} - e_u^O = e_v^T - e_u^O \quad (u=0,1,\ldots,6, v=0,1,\ldots,4). \tag{7}$$

The tetrahedral site energy e_v^T can be calculated by the embedded cell method. Here, the embedded clusters are tetrahedral clusters, i.e., $A_{4-v}B_v$. The calculated results of tetrahedral site energies e_v^T in the Nb-Ti-O system are shown in Fig. 8. This is also the result of the saddle-point energy of the oxygen Snoek relaxation in Nb-Ti alloys.

It is worth noting that adjacent octahedral clusters may have multiform spatial configurations, therefore, one kind of transition ($I_u^O \rightarrow I_{u'}^O$) may possess different activation energies ($H_{uu'}$) for different saddle-point status. For example, for the jump of interstitial atoms between two adjacent clusters A_5B, i.e., $I_1^O \rightarrow I_{1'}^O$, there are two possible configurations as shown in Fig. 9. It can be seen that two different saddle-point sites could exist in this transition, and accordingly, the activation

TABLE III. Data used in the calculations of the octahedral site energy of oxygen interstitial atoms in Nb-Ti alloys.

	V_m $(cm^3/mol)^a$	Ω $(kJ/cm^3)^a$	D^a	Λ $(kJ/mol)^b$	σ^c
Nb	10.8	171	0.75	−50.1	0.15
β-Ti	10.6	95	0.76		

[a]From Ref. 28.
[b]From Ref. 37.
[c]From Ref. 35.

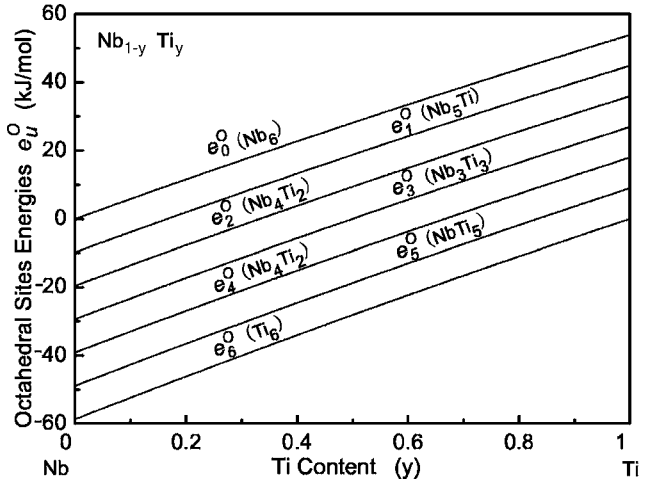

FIG. 5. The octahedral site energy e_u^O of oxygen atoms in Nb-Ti alloys as a function of alloy composition. Curves are calculated with the embedded-cell model.

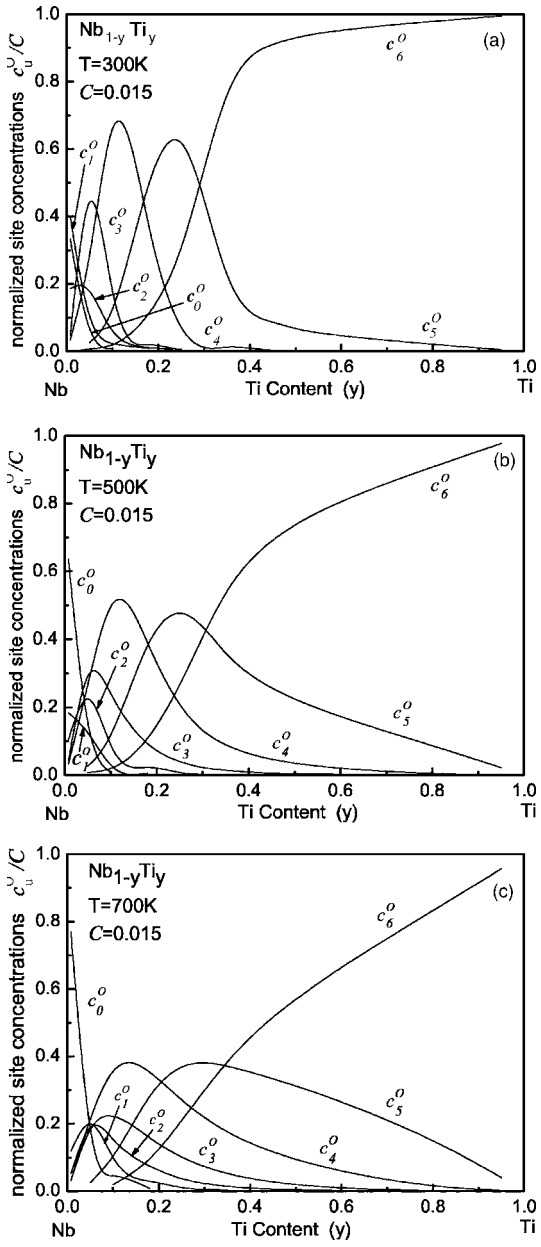

FIG. 6. The octahedral site concentration c_u^O of of oxygen atoms in Nb-Ti alloys at different temperatures: (a) at 300 K, (b) at 500 K, and (c) at 700 K.

energies should be $H_{11'}=e_0^T-e_1^O$ for case (a) and $H_{11'}=e_1^T-e_1^O$ for case (b), respectively. These different activation energies will lead to a scatter in the relaxation time τ_j and result in a broadening effect on the corresponding peak.

B. Transition probabilities of interstitial atoms and the Snoek relaxation

The probability[25,40] of a transition $I_u^O \rightarrow I_{u'}^O$ is proportional to c_u^O and to the fraction of adjacent sites $I_{u'}^O$ that can be occupied, that is to say, to a joint factor $\pi_{uu'}^O$ as given by

$$\pi_{uu'}^O = c_u^O q_{uu'}^O \left(1 - \frac{c_{u'}^O}{P_{u'}^O}\right). \tag{8}$$

where $1-c_{u'}^O/p_{u'}^O$ represents the conditional probability that, given an occupied site I_u^O, site $I_{u'}^O$ is not occupied.

The strength Δ of the overall relaxation[26] can be expressed as the sum of terms corresponding to all possible transitions between the adjacent interstitial sites of the various types, with each term's contribution being proportional to the corresponding jump probability factor $\pi_{uu'}^O$, i.e.,

$$\Delta = \sum_u K_{uu'} \pi_{uu'}^O, \tag{9}$$

where the coefficient $K_{uu'}$ represents the relaxation strength of a unit transition.

The temperature dependence of a Snoek relaxation, which contains several elementary Debye processes, can be described by the following expression:[41]

$$Q^{-1}(T) = \sum_u K_{uu'} \pi_{uu'}^O \sec h\left[\frac{H_{uu'}}{R}\left(\frac{1}{T} - \frac{1}{T_{muu'}}\right)\right], \tag{10}$$

where $H_{uu'}$ is activation energy for the jumping of $I_u^O \rightarrow I_{u'}^O$, which can be calculated by Eq. (7). $T_{muu'}$ is the peak temperature of the corresponding jump. Wert and Marx[42] have shown a linear correlation between $H_{uu'}$ and $T_{muu'}$ for Snoek-like peaks,

$$H_{uu'}(T_{muu'}) = RT_{muu'} \ln\left(\frac{kT_{muu'}}{hf_m}\right) + T_{muu'}\Delta S, \tag{11}$$

where k and h are the Boltzmann and Plank constants, ΔS is the entropy of the activation process, and f_m is the measuring frequency.

From Eqs. (8)–(11), a Snoek relaxation peak in a ternary bcc system could be calculated in principle, and on the other hand, a complex anelastic experimental result could be resolved into elementary anelastic processes. These elementary processes should be the natural mechanism of the whole Snoek profile. Here, we apply this method to analyze the Snoek relaxation mechanism of Nb-Ti-O alloys.

IV. EXPERIMENT AND DISCUSSION

A. Materials and data treatment procedures

Nb and Ti metals with a purity of 99.99% were used, and the alloy ingots were prepared in an argon-levitation melting furnace with a cold crucible. The prepared Nb-Ti alloy ingots were then segmented and remelted by the addition of TiO_2 powder in order to obtain the desired Nb-Ti-O alloys. Two different Nb-Ti-O systems were used in the present investigation: Nb-0.75Ti-1.5O and Nb-74Ti-1.5O (at. %).

Beam-shaped samples of dimensions $1\times10\times60$ mm^3 were used for relaxation spectra (Q^{-1}) measurements on a dynamic mechanical analyzer (DMA-2980, TA Instrument, Inc.). A forced vibration in the dual-cantilever mode was applied to the samples. The measuring temperature range was set from 10 to 450 °C at a heating rate of 2 °C/min and

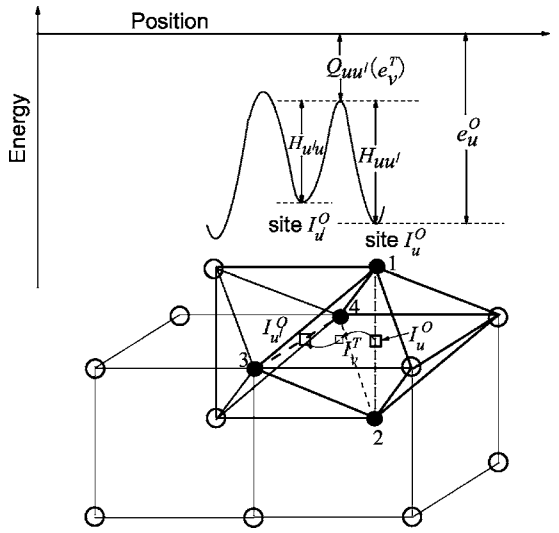

FIG. 7. The potential-energy diagram for interstitial solute atoms migrating over adjacent octahedral sites. The saddle-point energy of migrating ($Q_{uu'}$) appears at the tetrahedral interstitial site I_v^T between two adjacent octahedral sites (I_u^O and $I_{u'}^O$). This tetrahedral site is surrounded by four nearest-neighbor lattice atoms (respectively denoted by 1, 2, 3, and 4), which are shared by adjacent octahedral cell.

the frequency was set at 1 Hz. An exponentially formed background internal fraction was corrected according to the conventional method.[43]

The division of the temperature-dependence relaxation curves into constitutive Debye peaks was realized in Eq. (10) by specifying a set of reliable parameters: the transition probability $\pi_{uu'}^O$, the activation energy $H_{uu'}$, and the peak temperature $T_{muu'}$. These parameters were calculated by Eqs. (7), (8), and (11), while the factor $K_{uu'}$, as the fitting parameter, was varied until the best fit to the experimental curve was achieved. Then, a series of elementary peaks could be obtained corresponding to the possible elementary transitions $I_u^O \rightarrow I_{u'}^O$. For the entropy of activation, $\Delta S = 1.1 \times 10^{-4}$ eV/K was usually used as it gave the best matching of single experiments with those carried out by the Arrhenius plot for the Debye relaxation.[44] The Peak Fitting Module of the Microcal Origin program was used in the fitting procedures.

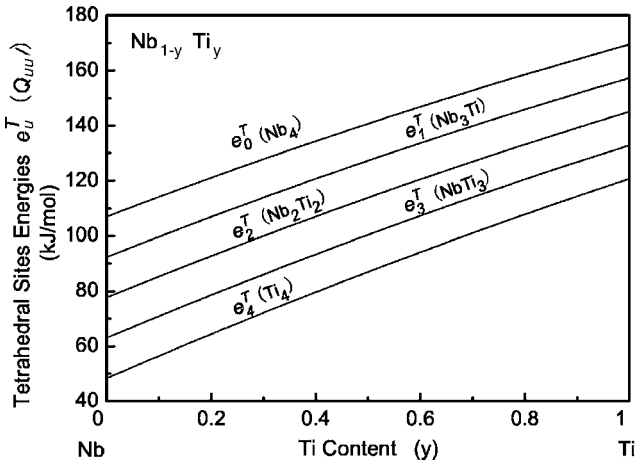

FIG. 8. Tetrahedral site energy e_v^T of oxygen atoms in Nb-Ti alloys. This energy is also treated as the saddle-point energy $Q_{uu'}$ for oxygen atom migration.

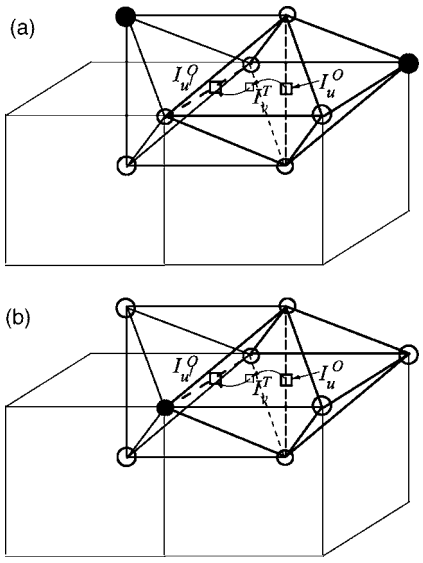

FIG. 9. Different possible spatial configurations for the transition type of $I_1^O \rightarrow I_{1'}^O$ in ternary system $A_{1-y}B_y$: (a) no substitutional atom B is shared by adjacent octahedral clusters and (b) one substitutional atom B is shared. Accordingly, they have different activation energies. ●—B atoms, ○—A atoms.

B. Experimental and fitting results

1. Nb-0.75Ti-1.5O (at. %)

In this system, oxygen atoms mainly distribute in three octahedral interstitial sites: I_0^O in the cell Nb_6, I_1^O in the cell Nb_5Ti, and I_2^O in the cell Nb_4Ti_2. Based on the analysis of spatial correlation as shown in Sec. II, there are six possible types of transitions between these interstitial sites: $I_0^O \leftrightarrow I_0^O$, $I_0^O \leftrightarrow I_1^O$, $I_0^O \leftrightarrow I_2^O$, $I_1^O \leftrightarrow I_1^O$, $I_1^O \leftrightarrow I_2^O$, and $I_2^O \leftrightarrow I_2^O$. As previously mentioned, some transitions may possess several spatial configurations. All possible spatial configurations and the parameters of these transitions are listed in Table IV.

Ten possible elementary transitions can be defined in this system. However, four of them, $I_1^O \leftrightarrow I_1^O$(I), $I_1^O \leftrightarrow I_2^O$(I), $I_2^O \leftrightarrow I_2^O$(I), and $I_2^O \leftrightarrow I_2^O$(III), can be neglected due to their poor transition probability. The main contribution to the total relaxation performance should be from the rest of the six transition processes. Accordingly, by fitting the shape of the experimental results, six elementary peaks can be determined. The fitting results are presented in Fig. 10. The dashed lines represent the six relaxation processes proposed, and the full line corresponds to the sum of relaxation process. This figure shows that the fitting curve has an essentially good coincidence with the experimental points. The area fraction $A_{uu'}$ of each elementary relaxation process, normalized to the whole area encompassed by the experimental points, is shown in Fig. 11. It can be seen that the $I_0^O \leftrightarrow I_1^O$ and $I_0^O \leftrightarrow I_0^O$ transitions were the main relaxation processes in

TABLE IV. The configurations and the relaxation parameters of all possible transitions of oxygen solute atoms in Nb-0.75Ti-1.5O (at. %) alloys. (○—Nb atoms and ●—Ti atoms.)

Transition type	Configuration	Transition Probability $\pi^O_{uu'} \Big/ \sum_u \pi^O_{uu'}$ (Normalized)	Site energy e^O_u (kJ/mol)	Saddle-point energy $Q_{uu'}(e^T_v)$ (kJ/mol)	Activation energy $H_{uu'}$ (kJ/mol)	Peak temperature $T_{muu'}$ (K)
$I_0^O \leftrightarrow I_0^O$	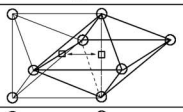	0.4361	0.44	107.45	107.01	430
$I_0^O \leftrightarrow I_1^O$	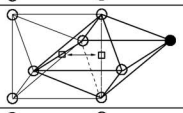	0.1746	-9.33	107.45	116.78	469
$I_0^O \leftrightarrow I_2^O$	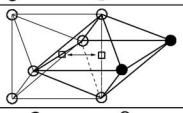	0.0155	-19.10	107.45	126.55	512
$I_1^O \leftrightarrow I_1^O$ I	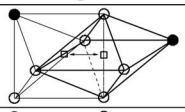	1.23×10^{-4}	-9.33	107.45	116.78	469
$I_1^O \leftrightarrow I_1^O$ II	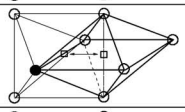	0.1746	-9.33	92.37	101.70	409
$I_1^O \leftrightarrow I_2^O$ I	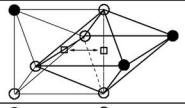	9.98×10^{-5}	-19.10	107.45	126.55	512
$I_1^O \leftrightarrow I_2^O$ II	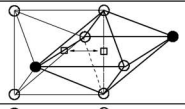	0.1215	-19.10	92.37	111.47	447
$I_2^O \leftrightarrow I_2^O$ I	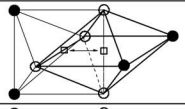	2.61×10^{-6}	-19.10	107.45	126.55	512
$I_2^O \leftrightarrow I_2^O$ II	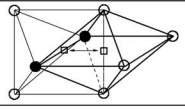	0.0765	-19.10	77.29	96.39	389
III	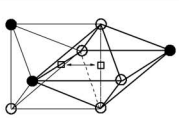	9.95×10^{-4}	-19.10	92.37	111.47	447

the Snoek effect of the Nb-0.75Ti-1.5O (at. %) alloys. The area fractions of both processes are as high as 45.31% and 20.73%, respectively.

It is worth noting that two elementary peaks at temperatures below the normal Snoek peak P($I_0^O \leftrightarrow I_0^O$) were fitted in this procedure: P[$I_1^O \leftrightarrow I_1^O$(II)] and P[$I_2^O \leftrightarrow I_2^O$(II)], respectively. These peaks should be due to interactions between oxygen atoms and the single or pairs of substitutional Ti solutes which are shared by the adjacent octahedral cell. This phenomenon was also observed in Fe-Mn(Cr)-N alloys,[11] and was qualitatively interpreted as arising from interstitial solutes trapped to pairs of substitutional atoms. Here, these elementary relaxation processes can be distinctly resolved and related to the concrete relaxation mechanism.

2. Nb-74Ti-1.5O (at. %)

In this alloy, oxygen atoms mainly distribute in the I_6^O and I_5^O sites (as shown in Fig. 6). Only at higher temperatures, minor parts of the oxygen will redistribute into the I_4^O site. Therefore, the transition situation of oxygen atoms in this alloy is simpler than the case of the Nb-0.75Ti-1.5O (at. %) system. Four main transition configurations and their corresponding parameters are listed in Table V. Here, we use these four elementary processes to resolve the experimental curve. The fitting results and the area fractions of each elementary peak are shown in Figs. 12 and 13, respectively. These results show that the main relaxation effects in this alloy should be due to the transitions of $I_5^O \leftrightarrow I_5^O$(II) and $I_6^O \leftrightarrow I_6^O$.

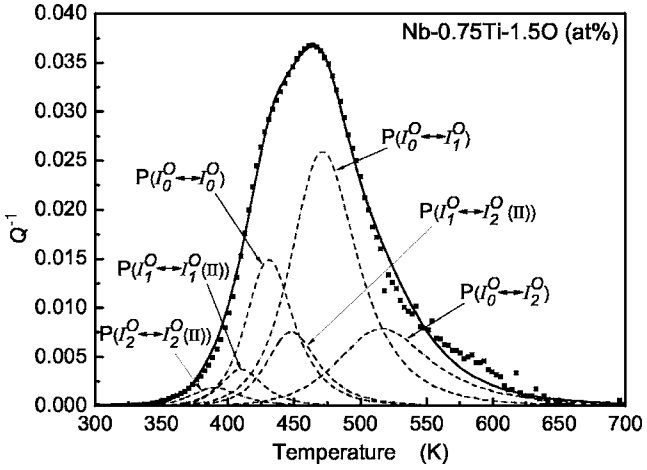

FIG. 10. Temperature dependence of the internal friction (at 1 Hz) and the fitting results in Nb-0.75Ti-1.5O (at. %) alloys (points—experimental, dashed line—fitted elementary peaks, and solid line—the sum of the elementary peak).

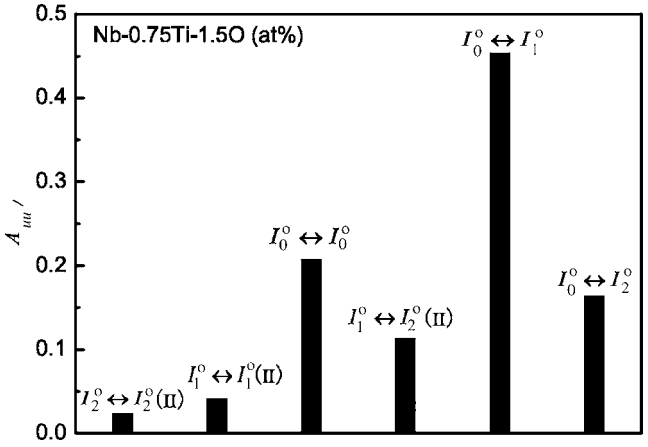

FIG. 11. The area fraction $A_{uu'}$ (normalized to the whole area encompassed by the experimental points in Fig. 10) of each elementary relaxation peak in Nb-0.75Ti-1.5O (at. %) alloys.

C. Discussion

In view of the complex spatial configurations of the lattice structure and the energy factors in an actual ternary system, a great number of elementary relaxation processes are theoretically possible. Some of these processes may be undetectable experimentally, and in some extreme cases they may only contribute to an increase of background dissipation. Biscarini *et al.* have proposed a qualitative expression to deal with this problem,[26] but this objective was not explicitly pursued. The present investigation achieved this goal in the ternary Nb-Ti-O alloys. Based on the theoretical analysis of the possible elementary jumps, a complex anelastic experimental result was resolved into effective elementary anelastic processes. In addition, these elementary relaxation processes can also be used as local probes for the physical and chemical structures of ternary bcc alloys.

As has been mentioned, the physical meaning of $K_{uu'}$ is the relaxation strength of a unit transition. The fitting values of $K_{uu'}$ of both systems are shown in Figs. 14(a) and 14(b), respectively. As a comparison, the transition probabilities $\pi^O_{uu'}/\Sigma_u \pi^O_{uu'}$ of the corresponding elementary peaks are also listed. One can see that for an elementary peak: (1) no direct relation exists between $K_{uu'}$ and $\pi^O_{uu'}$, (2) the values of $K_{uu'}$ are notably different for different peaks, and (3) a higher activation-energy elementary peak always has a higher $K_{uu'}$.

TABLE V. The configurations and the relaxation parameters of the main transitions of oxygen solute atoms in Nb-74Ti-1.50 (at. %) alloys. (○—Nb atoms and ●—Ti atoms.)

Transition type	Configuration	Transition probability $\pi^O_{uu'}/\sum_u \pi^O_{uu'}$ (Normalized)	Site energy e^O_u (kJ)	Saddle-point energy $Q_{uu'}(e^T_v)$ (kJ)	Activation energy $H_{uu'}$ (kJ/mol)	Peak temperature $T_{muu'}$ (K)
$I_4^O \leftrightarrow I_4^O$	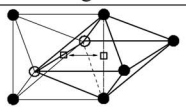	0.0096	4.03	130.34	126.31	504
$I_5^O \leftrightarrow I_5^O$	I 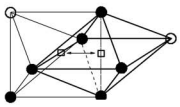	0.0644	-5.21	103.88	109.09	437
	II 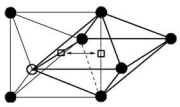	0.0944	-5.21	118.27	123.48	493
$I_6^O \leftrightarrow I_6^O$	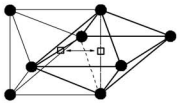	0.6887	-14.52	104.08	118.60	474

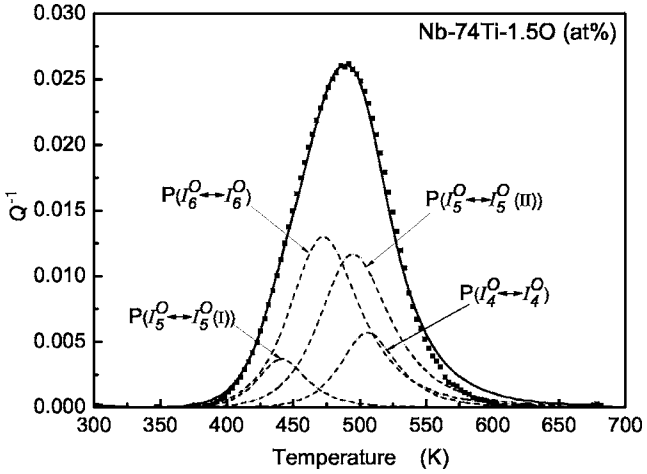

FIG. 12. Temperature dependence of internal friction (at 1 Hz) and the fitting results in Nb-74Ti-1.5O (at. %)alloys (points—experimental, dashed line—fitted elementary peaks, and solid line—the sum of the elementary peak)

It is well known that the strength of the Snoek relaxation mainly depends on the interstitial solute concentration, the anisotropy of the strain field around the interstitial solute atom[14] and the symmetry characteristics of the point-defect reorientation. Recalling Eqs. (8) and (9), the influence of the interstitial atom concentration has been considered in the factor $\pi_{uu'}^O$. The strain field of the oxygen interstitial atoms can be treated as a constant in different elementary relaxation processes in the Nb-Ti-O system since Nb and Ti have similar atomic radii. Therefore, the fitting parameter $K_{uu'}$ mainly reflects the symmetry-related responses of the interstitial solute reorientation in the relaxation process. In principle, the symmetry characteristics of point-defect reorientation can be calculated using the elastic-dipoles selection rules suggested by Nowick and Berry[1] and Nowick and Heller.[15] However, this is an inconvenient method since there are many unknown parameters and numerous possible spatial correlations, and it needs to be tackled case by case. Some extremely simple cases can be experimentally measured under

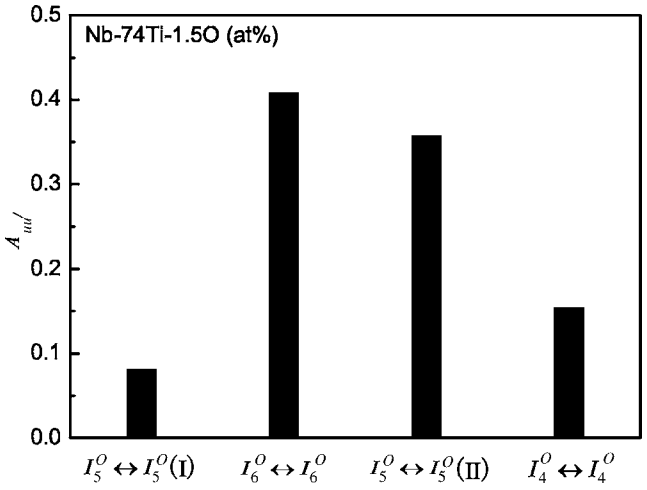

FIG. 13. The area fraction $A_{uu'}$ of each elementary relaxation peak in Nb-74Ti-1.5O (at. %) alloys.

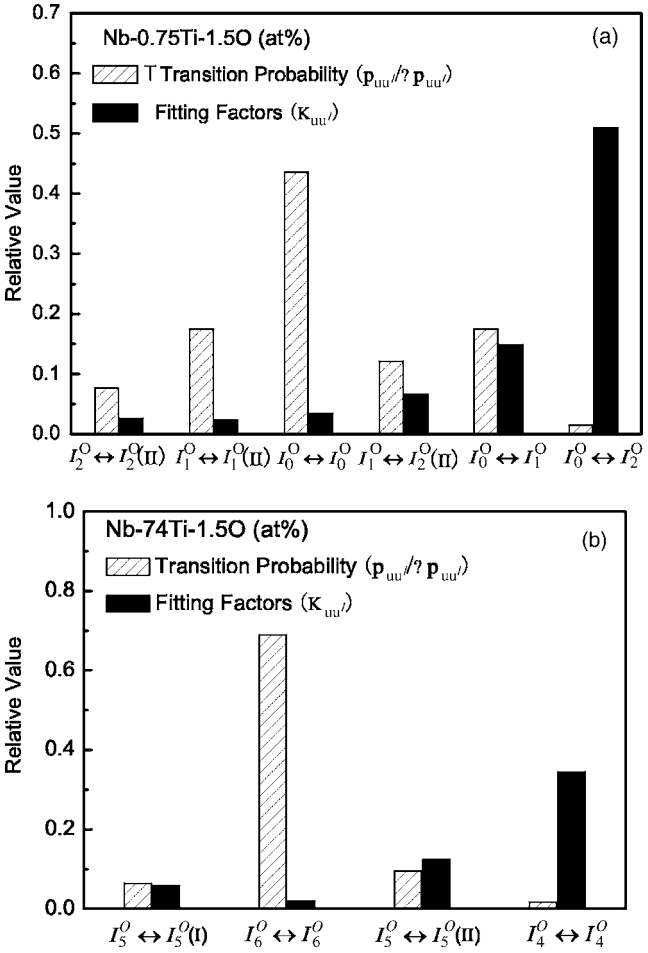

FIG. 14. The fitting values of $K_{uu'}$ of each elementary peaks in both alloys: (a) Nb-0.75Ti-1.5O and (b) Nb-74Ti-1.5O (at. %).

single-crystal conditions. Here, this information can be obtained, at least relatively, by using the fitting results of the factor $K_{uu'}$.

To a certain extent, the contribution of an elementary process to the overall relaxation effects mainly depends on the factor $K_{uu'}$, rather than the transition probability. For example, in Nb-0.75Ti-1.5O (at. %) alloys, the main jumps of interstitial oxygen atoms occur in the process $I_0^O \leftrightarrow I_0^O$; however, the main relaxation contribution results from the process $I_0^O \leftrightarrow I_1^O$, since the latter has a higher factor $K_{uu'}$. Therefore, the factor $K_{uu'}$ can be used to analyze and compare the validity among the elementary relaxation processes.

As shown in Fig. 14, the transition types of $I_0^O \leftrightarrow I_2^O$ and $I_4^O \leftrightarrow I_4^O$ are the most effective relaxation processes in the present two alloys. Both of these transitions have the same symmetry characteristics of their reorientation responses; i.e., prior to and after the transitions, they change from the symmetrical about ⟨1 0 0⟩ to the symmetrical about ⟨0 1 0⟩. It implies that such reorientation could induce the largest relaxation effect. This result can also be applied in the design of high-damping alloys. High damping performance could be obtained by the selection of the alloy components and the controlling of ordering structure,[45] which can cause the distribution and the transition of the major interstitial atoms in the most effective relaxation processes.

V. CONCLUSIONS

An extended statistical mechanical model, combined with a fitting method, has been proposed to resolve the complicated Snoek relaxation peak in ternary bcc system.

(1) The interstitial site occupancies, the spatial site configurations and the transition probabilities of the octahedral interstitial solute atoms were calculated in detail using an embedded-cell model, assuming the energy of the interstitial atoms to be predominantly determined by the nearest-neighbor metal atoms. Based on these information, all possible elementary processes of the Snoek relaxation in ternary bcc system can be predicted.

(2) Following the embedded-cell model, both octahedral and tetrahedral site energies of the interstitial atoms in these elementary relaxation processes were calculated. The results were used to estimate the activation energy and the peak temperature of the corresponding elementary relaxation process. Then, using a fitting method, the complicated Snoek spectrums were resolved into several effective elementary Debye peaks, which correspond to the concrete relaxation mechanism.

(3) This method has been successfully applied to analyze the complex Snoek peak in Nb-Ti-O alloys. The fitting results shown that the most notable relaxation process occurs in the reorientation response in which the symmetry characteristic changes from the symmetrical about $\langle 1\ 0\ 0\rangle$ to about $\langle 0\ 1\ 0\rangle$ prior to and after the oxygen transition.

(4) This method can be used to describe the Snoek relaxation behavior in ternary bcc systems.

[1] A. S. Nowick and B. S. Berry, *Anelastic Relaxation in Crystalline Solids* (Academic, New York, 1972), Chaps. 9 and 11.
[2] H. Numakura and M. Koiwa, J. Phys. IV **6**, C8–97 (1996).
[3] T. G. Chen, C. Jiang, and Z. L. Wu, J. Phys. **46**, C10–39 (1985).
[4] M. S. Blanter and M. Y. Fradkov, Acta Metall. Mater. **40**, 2201 (1992).
[5] R. W. Powers and M. V. Doyle, Acta Metall. **4**, 233 (1956).
[6] M. S. Ahmad and Z. C. Szkopiak, J. Phys. Chem. Solids **31**, 1799 (1970).
[7] G. Gibala and C. A. Wert, Acta Metall. **14**, 1095 (1966).
[8] F. W. J. Botta, O. Florencio, C. R. Grandini, H. Tejima, and J. A. R. Jordao, Acta Metall. Mater. **38**, 391 (1990).
[9] O. Florencio, F. W. J. Botta, C. R. Grandini, H. Tejima, and J. A. R. Jordao, J. Alloys Compd. **211/212**, 37 (1994).
[10] L. J. Dijkstra and R. J. Sladek, Trans. AIME **197**, 69 (1953).
[11] I. G. Ritchie and R. Rawlings, Acta Metall. **15**, 491 (1967).
[12] Z. C. Szkopiak and J. T. Smith, J. Phys. D **8**, 1273 (1975).
[13] R. Cantelli and Z. C. Szkopiak, Appl. Phys. **9**, 153 (1976).
[14] H. Numakura, G. Yotsui, and M. Koiwa, Acta Metall. Mater. **43**, 705 (1995).
[15] A. S. Nowick and W. R. Heller, Adv. Phys. **12**, 251 (1963).
[16] M. Koiwa, Philos. Mag. **24**, 81 (1971); **24**, 107 (1971); **24**, 539 (1971); **24**, 799 (1971).
[17] E. Miura, K. Ota, K. Yoshimi, and S. Hanada, Philos. Mag. **83**, 2343 (2003).
[18] N. P. Kushnareva, S. E. Snejko, and I. P. Yarosh, Acta Metall. Mater. **43**, 4393 (1995).
[19] N. P. Kushnareva and S. E. Snejko, J. Alloys Compd. **211/212**, 75 (1994).
[20] D. Mosher, C. Dollins, and C. Wert, Acta Metall. **18**, 797 (1970).
[21] P. Gondi and R. Montanari, Phys. Status Solidi A **131**, 465 (1992).
[22] I. S. Golovin, J. Alloys Compd. **310**, 356 (2000).
[23] S. Alberici, R. Montanari, and M. E. Tata, J. Alloys Compd. **310**, 209 (2000).
[24] A. A. Sagues and R. Gibala, Scr. Metall. **5**, 689 (1971).
[25] A. Biscarini, B. Coluzzi, and F. M. Mazzolai, Acta Mater. **47**, 3447 (1999).
[26] A. Biscarini, B. Coluzzi, and F. M. Mazzolai, Defect Diffus. Forum **165–166**, 1 (1999).
[27] R. C. Brouwer, E. Salomons, and R. Griessen, Phys. Rev. B **38**, 10217 (1988).
[28] R. C. Brouwer and R. Griessen, Phys. Rev. B **40**, 1481 (1989).
[29] R. C. Brouwer, J. Rector, N. Koeman, and R. Griessen, Phys. Rev. B **40**, 3546 (1989).
[30] R. B. McLellan, Acta Metall. **30**, 317 (1982).
[31] K. Alex and R. B. McLellan, J. Phys. Chem. Solids **32**, 449 (1971).
[32] R. Griessen, Phys. Rev. B **27**, 7575 (1983).
[33] Z. C. Szkopiak, J. Phys. (Paris) **32**, C2–1 (1971).
[34] F. X. Yin, S. Iwasaki, D. H. Ping, and K. Nagai, Adv. Mater. (Weinheim, Ger.) **18**, 1541 (2006).
[35] P. S. Rudman, Acta Metall. **12**, 1381 (1964).
[36] R. Kirchheim, Defect Diffus. Forum **143–147**, 911 (1997).
[37] R. J. Lauf and C. J. Altstetter, Acta Metall. **27**, 1157 (1979).
[38] T. C. Niemeyer, C. R. Grandini, and O. Florencio, Mater. Sci. Eng., A **396**, 285 (2005).
[39] D. E. Jiang and E. A. Carter, Phys. Rev. B **67**, 214103 (2003).
[40] B. Coluzzi, C. Costa, A. Biscarini, and F. M. Mazzolai, J. Phys.: Condens. Matter **4**, 53 (1992).
[41] A. Puskar, *Internal Friction of Materials* (Cambridge International Science, Cambridge, 2001), Chap. 3.
[42] C. Wert and J. Marx, Acta Metall. **1**, 113 (1953).
[43] M. S. Ahmad, D. E. Barrow, E. A. Little, and Z. C. Szkopiak, J. Phys. D **4**, 1460 (1971).
[44] I. S. Golovin, H. Neuhauser, and A. Riviere, Intermetallics **12**, 125 (2004).
[45] S. Shang and A. J. Bottger, Acta Mater. **51**, 3597 (2003).